Macromolecular Materials and Engineering
www.mme-journal.de

Phosphorus-Containing Polymer Flame Retardants for Aliphatic Polyesters

*Madeleine Schwarzer, Andreas Korwitz, Hartmut Komber, Liane Häußler, Bettina Dittrich, Bernhard Schartel, and Doris Pospiech**

Polyesters with 9,10-dihydro-9-oxy-10-phosphaphenanthrene-10-oxide-containing comonomers are synthesized aiming to improve the flame retardancy of aliphatic polyesters such as poly(butylene succinate) and poly(butylene sebacate). The influence of the chemical structure on the thermal decomposition and pyrolysis is examined using a combination of thermogravimetric analysis (TGA), TGA-Fourier transform infrared (FTIR) spectroscopy, pyrolysis-gas chromatography/mass spectrometry, and microscale combustion flow calorimetry. Thermal decomposition pathways are derived and used to select suitable candidates as flame retardants for PBS. The fire behavior of the selected polymers is evaluated by forced-flaming combustion in a cone calorimeter. The materials show two modes of action for flame retardancy: strong flame inhibition due to the release of a variety of molecules combined with charring in the solid state.

1. Introduction

Biobased polymers, that is, polymers that are prepared or originate from biological sources, have recently gained an increasing interest to improve sustainability in the plastics industry. A number of biobased, but synthetic polymers have already been successfully introduced, for instance, poly(lactic acid), poly(hydroxybutyrate) and their copolymers, thermoplastic starch, isosorbide-based resins, poly(ethylene furanoate) (PEF),[1,2] and poly(glycerol sebacate) acid stearate polymers.[3] Poly(butylene succinate) (PBS)[4] and its copolymers[5] were introduced besides PEF as alternative to the classical polyesters, poly(ethylene terephthalate) (PET) and poly(butylene terephthalate) (PBT), for engineering applications. PBS shows attractive properties: good processability, interesting mechanical performance, and a high heat deflection temperature of about 97 °C combined with a moderate degree of biodegradability.[6,7] This property attracts more and more attention because of the potential that it offers for the long-term reduction in pollution of the environment with microplastics of high durability.[8] Many applications use copolyesters with poly(butylene sebacate) (P(B-Seb)) segments. PBS and P(B-Seb) are aliphatic polyesters and owing to their chemical structure they are easily thermally degradable and combustible with high heat release capacity and flammability.[9] For these new materials, the development of effective, halogen-free flame retardants (FRs) according to the European regulations WEEE 2012/19/EU (Waste of Electrical and Electronic Equipment) and REACH is still a challenging and continuing task.[10,11] The addition of FR either as an additive or incorporated into the polyester chain is unavoidable. One possibility is the use of organophosphorus compounds as additives which act both in the gas phase as well as in the condensed phase.[12–15] Addition of polymeric phosphorus-containing FRs provides a better incorporation into the polymer matrix and avoids leaching. A number of phosphorus-containing polymers with varied chemical structure have been developed and proposed as FR additives[6,11,16–23] for polyesters. Most of these polymers contain 9,10-dihydro-9-oxy-10-phosphaphenanthrene-10-oxide (DOPO) substituents attached to the polyester main chain.

In previous attempts to improve the flame retardancy of aliphatic polyesters, DOPO substituents were connected to a hydroquinone core and the core was glycolized to form the diol monomer DOPO-HQ-GE (10-[2,5-bis(2-hydroxyethoxy)-phenyl]-9,10-dihydro-9-oxa-10-pospha-phenanthrene-10-oxide; alternative name: 2,2′-[[2-(6*H*-dibenz[*c*,*e*][1,2]-oxaphosphorin-6-yl)-1,4-phenylene]-bis(oxy)] bis[ethanol])).[19] The resulting polyester with terephthaloyl units (polymer from dimethyl terephthalate and DOPO-HQ-GE, named in this work P(P-T)) showed high flame retardancy potential with a balance between gas phase action, condensed phase action, and intumescence,[24] and worked well as a flame retardant in PBT.[14] However, P(P-T) is not optimal as a FR for aliphatic polyesters because its softening range is too high, due to the T_g of 146 °C, and does not match the melting range of aliphatic polyesters.[9] Therefore, a series of new polyesters and copolyesters with the DOPO adduct to dimethylitaconate (2-(6-oxido-6*H*-dibenz [*c*,*e*][1,2] oxaphosphorin-6-yl) dimethyl itaconate, ItaP)) was designed and examined. The synthesis of ItaP was adapted from a previously reported procedure.[9,25,26]

M. Schwarzer, A. Korwitz, Dr. H. Komber, L. Häußler, Dr. D. Pospiech
Leibniz-Institut für Polymerforschung Dresden e. V.
Hohe Str. 6, 01069 Dresden, Germany
E-mail: pospiech@ipfdd.de
Dr. B. Dittrich, Dr. B. Schartel
Bundesanstalt für Materialforschung und -prüfung (BAM)
Unter den Eichen 87, 12205 Berlin, Germany

DOI: 10.1002/mame.201700512

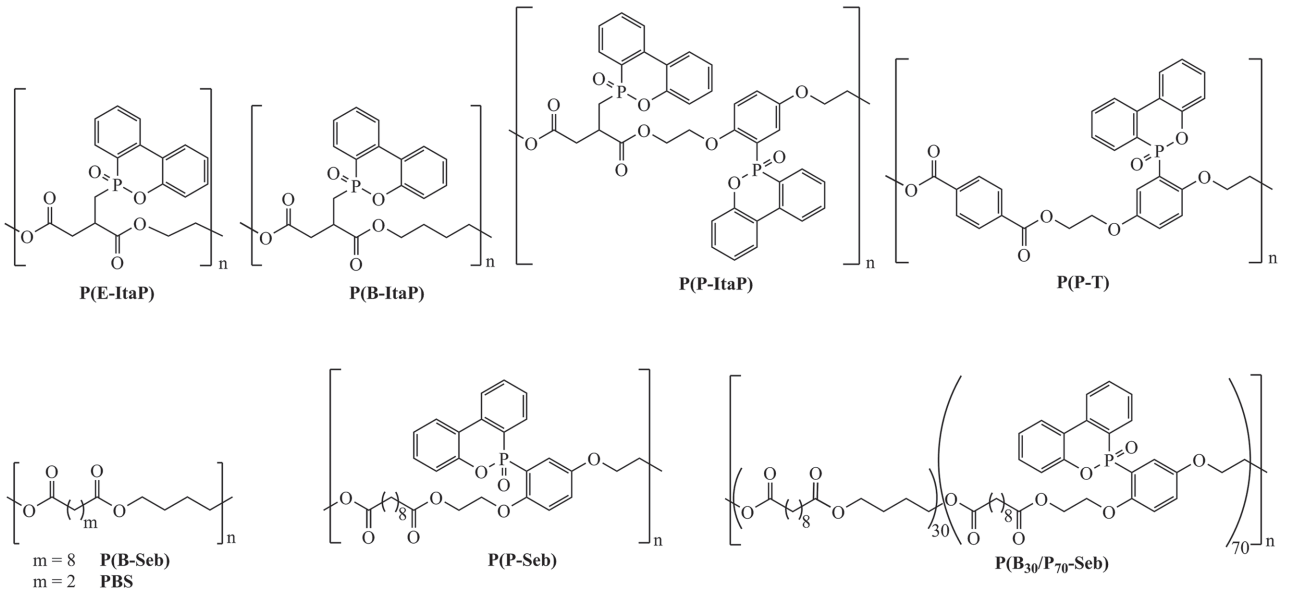

Figure 1. Chemical structures of the synthesized polyesters.

Here, the synthesis and properties of a series of polyesters based on PBS and P(B-Seb) are reported. The chemical structures of the polyesters studied are illustrated in **Figure 1**. The main focus was to examine the decomposition and fire behavior of the materials as a function of chemical structure to find conclusions about the decomposition pathway. A further aim was to evaluate the potential of the materials as flame retardants for PBS in comparison to the phosphorus-polyester P(P-T) to understand the differences between itaconate-based DOPO polyesters and terephthalate-based DOPO polyesters. To achieve that, a combination of thermogravimetric analysis (TGA), TGA coupled with Fourier-transform infrared (FTIR) spectroscopy (TGA-FTIR), and pyrolysis-gas chromatography/mass spectrometry (Py-GC/MS) was employed.

Additionally, forced-flaming investigations in a cone calorimeter were carried out to explore the fire behavior of the materials and to estimate the potential as flame retardant additive.

2. Experimental Section

2.1. Materials

Antimony(III) oxide (Sb_2O_3, Aldrich, 99.9%, nanopowder), butane-1,4-diol (Acros Organics, Sigma-Aldrich, 99%, stored over molecular sieves), DOPO (TCI Europe, >97.0%), dimethyl itaconate (Acros Organics, 97%, stabilized), dimethyl sebacate (Sigma-Aldrich, ≥95%), dimethyl succinate (Acros Organics, 99%), ethylene glycol (Sigma-Aldrich, 99.8%, anhydrous, stored over molecular sieves), hydroquinone bis(2-hydroxyethyl) ether (Aldrich, 98%), polyethylene terephthalate (DSM, PET Arnite D04300), propane-1,3-diol (VWR international, 99.7%), magnesium sulfate (Sigma-Aldrich, 97%, anhydrous), sodium bicarbonate (Fluka, ≥99%), titanium(IV) *n*-butoxide ($Ti(BuO)_4$, Acros Organics, 99%, stored under nitrogen), and Ukanol ES (Schill + Seillacher GmbH, Heidenau, 69%) were used as received. Dimethyl terephathalate (Acros Organics, 99%) was recrystallized twice from ethanol. DOPO-itaconate was synthesized from dimethyl itaconate and DOPO as previously reported.[9,25,26] The preparation of DOPO-HQ-GE from DOPO-hydroquinone was carried out as previously described.[19,27,28]

2.2. Polycondensations

A 2.3 L stirring autoclave was dried at 120 °C under nitrogen overnight. Then, it was filled with the monomers, that is, the respective dicarboxylic acid dimethyl ester and the respective diol (molar ratio dimethyl ester/diol = 1/2 in case of PET and P(E-ItaP) and 1/1.2 for all other polymers) as well as a mixture of $Ti(BuO)_4/Sb_2O_3$ (1 wt% each with respect to the initial weight of the dicarboxylic acid ester). In the case of PBS, PBT and P(B-Seb) just $Ti(BuO)_4$ were used as catalyst. After filling, the autoclave was purged three times, and the temperature was raised under a moderate stream of nitrogen. The reaction mixture was heated to 200 °C, whereby the reactants melted. The temperature was further raised with a heating rate of 2 K min^{-1} to 245 °C and stirred for further 30 min at 245 °C under moderate stream of nitrogen, with 60 rpm. Then, the reaction mixture was stirred for 4–7 h (depending on the monomers used) at 245 °C under vacuum. After the reaction completed, the autoclave was cooled down and the completely cooled product was removed mechanically. The yields of the cream-colored to black products amounted to 42–95%. During the entire reaction, the autoclave parameters (torque, pressure, and temperature) were monitored. The polyesters were characterized by solution viscosity, ^1H, ^{13}C, and ^{31}P NMR (nuclear magnetic resonance) spectroscopy and size exclusion chromatography (SEC).

2.3. Measurements

2.3.1. Size Exclusion Chromatography

SEC was performed in a modular SEC consisting of an HPLC-pump (Series 1200, Agilent Technologies, USA), separation column PL MiniMIX-D (Agilent Technologies, USA), differential refractometer (KNAUER, Germany), and an RI detector using pentafluorophenol/chloroform (PFP/$CHCl_3$) 33/67 (vol/vol) as eluent with a flow rate of 0.3 mL min^{-1} at 45 °C. Narrow distributed polystyrene was used as standard for calibration.

2.3.2. Differential Scanning Calorimetry (DSC)

The DSC measurements were performed on a Q 2000 (TA Instruments, USA) in a temperature range from –80 to 250 °C at a scan rate of ±10 K min^{-1} with nitrogen as purge gas. The first heating, cooling, and second heating run were recorded. About 5 mg of sample were used.

2.3.3. Nuclear Magnetic Resonance Spectroscopy

The ^{1}H (500.13 MHz), ^{13}C (125.74 MHz), and ^{31}P (202.46 MHz) NMR spectra were recorded using an Avance III 500 NMR spectrometer (Bruker Biospin, USA) at 30 °C. For most of the samples, $CDCl_3$ was used as solvent, except for PBT, which was dissolved in a mixture of $CDCl_3$ and CF_3COOD 50/50 (vol/vol). The spectra were referenced on the solvent signal ($\delta(^{1}H)$ = 7.26 ppm; $\delta(^{13}C)$ = 77.0 ppm) or on external H_3PO_4 ($\delta(^{31}P)$ = 0 ppm).

2.3.4. Quantitative Phosphorus Content

The quantitative phosphorus content was determined by Mikroanalytisches Labor Kolbe (Höhenweg 17, D-45470 Mühlheim a.d. Ruhr, Germany).

2.3.5. Viscometry

The solution viscometry was determined by a SI Analytics CT 72/2 in a capillary I with pentafluorophenol/chloroform 50/50 (vol/vol) as eluent at 25 °C and with a concentration of 0.5 g polymer dL^{-1}.

2.3.6. Microscale Combustion Calorimetry

The pyrolysis was examined by MCC using a FAA Micro Calorimeter (Fire Testing technology Ltd., UK) within a temperature range from 75 to 750 °C and at a heating rate of 60 K min^{-1}. About 5 mg of sample were used.

2.3.7. Pyrolysis-Gas Chromatography Coupled with Mass Spectrometry

Py-GC/MS was performed with a modular system composed of a pyrolyzer Pyroprobe 5000 (CDS Analytical Inc., USA) with a platinum filament, a gas chromatograph GC7890A (Agilent Technologies, USA) with a HP-5MS-Säule (nonpolar, 30 m × 250 µm × 0.25 µm), and a mass spectrometer MSD 5975 CD inert XL EI/CD (EI at 70 eV, mass scan range 15–550 m/z, Agilent Technologies, USA). For the flash pyrolysis, the interface CDS1500 at 280 °C and a pyrolysis temperature at 600 °C (isotherm for 10 s) was used. The inlet temperature during gas chromatography was 280 °C and the oven temperature was first maintained isothermally at 50 °C for 2 min, increased to 280 °C with a gradient of 12 K min^{-1} and finally isothermally held at 280 °C for 10 min.

2.3.8. Thermogravimetric Analysis and Thermogravimetric Analysis Coupled with Fourier-Transform-Infrared Spectroscopy

TGA was carried out with a Q 5000 instrument (TA Instruments, USA) with a heating rate of 10 K min^{-1} in the temperature range of 40–800 °C using nitrogen as purge gas and a sample amount of about 15 mg. For TGA-FTIR investigation, the TGA device was used in conjunction with the FTIR spectrometer Nicolet 380. The method was carried out with 100 mL min^{-1} flow at a heating rate of 10 K min^{-1} to 800 °C. The evaluation of the TGA-FTIR spectra was done using software OMNIC 2.7.

2.3.9. Cone Calorimeter

A cone calorimeter (Fire Testing Technology, FTT, UK) was used to investigate the fire behavior under forced-flaming conditions according to ISO 5660. Specimens of 100 mm × 100 mm × 3 mm in size were measured in aluminum trays exposed to an irradiation of 50 kW m^{-2}. The cone heater-to-sample distance was 45 mm considering the strong bending of the sample plates prior to ignition.[29,30] All measurements were done only in duplicate, since the repeatability was satisfactory with less than 10% deviation in all of the fire properties. The values for total heat evolved (THE) and the residual mass were taken at the time to flame-out (t_{fo}) resulting in the total heat release at time to flame-out (THR(t_{fo})). Flame-out was defined as the extinguishment of the visible yellow flame plus 10 s making the results comparable for all measurements.

3. Results and Discussion

3.1. Polymer Synthesis Results

The initial chemical structure of PBT was systematically altered to study the influence of the aliphatic and aromatic monomer fractions in the polyesters. While in our first report aromatic-aliphatic (co)polyesters with DOPO-HQ-GE as diol linked to aliphatic dicarboxylic acids were discussed,[9] here 2-(6-oxido-6*H*-dibenzo[*c*,*e*][1,2]-oxazaphosphorin-6-yl-dimethyl itaconate (ItaP) was mainly used as phosphorus-containing monomer. Thus, the DOPO substituent was shifted from the diol to the dicarboxylic acid unit and this monomer replaced the terephthaloyl unit. The present study discusses the thermal decomposition, flammability, and fire behavior of polyesters

Table 1. Chemical characterization of the homo- and copolyesters synthesized.

Sample	SEC[a]			Solution viscosity	P-content		DSC
	M_n [g mol^{-1}]	M_w [g mol^{-1}]	M_w/M_n	η_{Inh} [dL g^{-1}]	Calculated [wt%]	Measured [wt%]	T_g [°C]
PBT[9]	32 000	76 800	2.40	0.90	0	0	45
PBS	143 400	276 800	1.93	1.90	0	0	–31
P(P-T)[19]	20 200	309 400	15.32	0.60	5.71	5.95	147
P(E-ItaP)	5000	15 700	3.12	0.30	8.32	7.95	80
P(B-ItaP)	13 100	26 000	1.98	0.21	7.74	7.74	62
P(P-ItaP)	14 200	102 100	7.19	0.26	8.57	8.01	125
P(B-Seb)	74 300	159 500	2.15	1.50	0	0	-53
P(P-Seb)	14 600	32 700	2.24	0.33	5.35	5.42	63
P(B_{30}/P_{70}-Seb)	37 400	133 600	3.57	0.83	3.75	4.29	n.a.

[a]Mass average and number average molar mass found by SEC relative to polystyrene standards; n.a.: not analyzed.

having ItaP as dicarboxylic acid unit including the comparison with PET, PBT, and P(B-Seb). Finally, a polyester with DOPO in both diol unit as well as dicarboxylic acid unit (P(P-ItaP)) was regarded as one possibility to raise the phosphorus content in the materials. Enhancing the P-content is an important issue to reduce the necessary content of phosphorus polyester as FR additive.

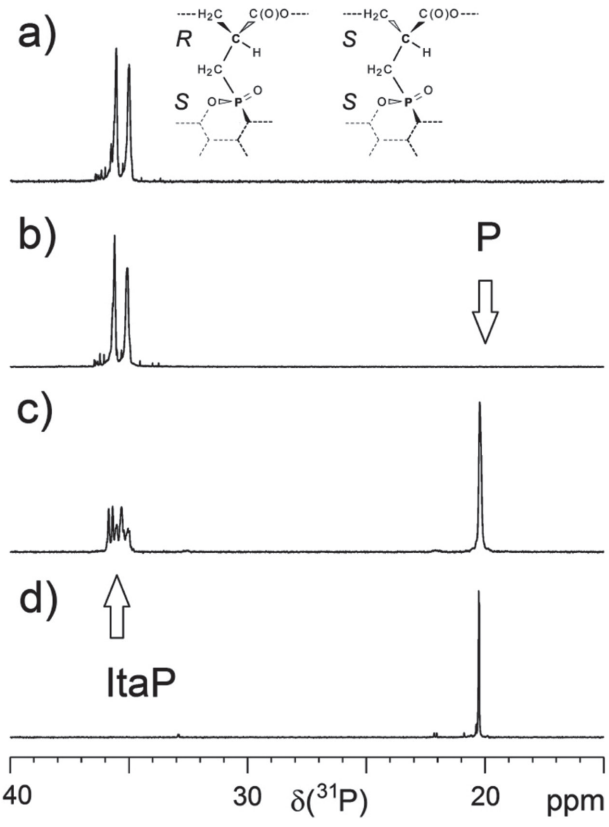

Figure 2. ^{31}P NMR spectra of a) P(E-ItaP), b) P(B-ItaP), c) P(P-ItaP), and d) P(P-Seb). Solvent: $CDCl_3$. The inset illustrates two diastereomers of the ItaP moiety.

Transesterification of the dimethyl esters of the dicarboxylic acids with aliphatic diols in the melt was employed for polycondensation. The synthesis of all polyesters was carried out under comparable conditions to achieve better comparability of the test results. The chemical characterizations of the polyesters obtained by SEC, viscometry, quantitative phosphorus content determination, and DSC are summarized in **Table 1**.

The relative molar masses of all polyesters were sufficiently high for evaluation of material properties. The molar mass M_n of PBS was about 150 000 g mol^{-1} and, thus, much higher than values previously reported, for example, in refs. [31,32]. But, it has to be noted that the relative values obtained should not be compared directly (also with values from literature) because the SEC conditions as well as the chemical structures and thus the corresponding Kuhn–Mark–Houwink parameters of the polymers are different. The solution viscosities η_{Inh} correlated with the number average molar masses M_n. The dispersities $Đ = M_w/M_n$ were in the typical range of step-growth polymerizations (≈2).[33] The experimental phosphorus contents were close to the calculated values. The highest phosphorus content was determined for P(P-ItaP) (8.01 wt%) with two DOPO-units. A detailed analysis of the chemical structure of the new polymers was performed by NMR spectroscopy.

3.2. Structural Characterization by NMR Spectroscopy

Besides well-known phosphorus-free polyesters and polyesters based on the DOPO-HQ-GE diol monomer (P), which have been characterized in detail in a preceding paper,[9] this study involves new polyesters based on the diastereomeric ItaP dicarboxylic acid comonomer. The NMR data and NMR spectra of P(E-ItaP), P(B-ItaP), and P(P-ItaP) are given in Figures S1–S6 (Supporting Information). ItaP dimethylester has two stereocenters (methine carbon and phosphorus) resulting in two diastereomers. They do not result in different NMR signals for the dimethyl ester[9] but in the polymers P(E-ItaP) and P(B-ItaP) two well-separated ^{31}P NMR signals were observed with $\Delta\delta \approx 0.5$ ppm (**Figure 2**a,b). This is different to P(P-Seb) (Figure 2d) based on P with only one stereocenter

(phosphorus). Because this nonsymmetric monomer can result in regioregularity effects (head and tail orientation; Scheme S1, Supporting Information)[9,20] and in stereosequences due to the asymmetric methine carbon, a model polyester P(D-ItaP) was synthesized with 1,12-dodecane diol (D) to clarify the reason for signal splitting. Here, the ItaP units are separated by 15 bonds which eliminate regioregularity and stereosequence effects on the NMR spectra (Figures S7–S10, Supporting Information). Thus, besides ^{31}P scalar couplings, only a diastereomeric effect can result in signal splitting. In fact, two ^{31}P NMR signals ($\Delta\delta$ = 0.6 ppm) and additional splittings for several ^{13}C NMR signals of the ItaP unit (up to $\Delta\delta \approx$ 0.6 ppm) and for the OCH_2 signals (0.05 ppm) were observed (Figure S9, Supporting Information). This proves that attention must be paid to this effect in the interpretation of ^{13}C NMR spectra. The complexity of the ^{1}H NMR spectra of all the polymers studied does not allow the identification of effects due to diastereomers, regioregularity, and stereosequences.

P(B-ItaP) is similar to the model polyester but contains the shorter butane diol. ^{1}H and ^{13}C NMR spectra confirm the expected structure (Figures S3 and S4, Supporting Information). The splitting of ^{13}C NMR signals of the ItaP unit matches that of the model polyester and can be attributed to the diastereomer effect. The corresponding $\Delta\delta$ values are smaller for aliphatic carbons but no additional splitting due to regioregularity or stereosequences was observed. The small splitting of the inner methylene carbon signals cannot be unequivocally assigned to one of these effects. For P(E-P-Ita), the NMR spectra point to the incorporation of ≈10–15 mol% diethylene glycol units in the backbone, which were formed by partial etherification of the ethyleneglycol comonomer (Figures S1 and S2, Supporting Information). Signal groups at 68.3 ppm (ether CH_2) and 63.6 ppm (ester CH_2) in the ^{13}C NMR spectrum and at 3.55 ppm (ether CH_2) in the ^{1}H NMR spectrum are characteristic for this moiety. This additional comonomer increases the complexity of the NMR spectra and a detailed analysis was not carried out. The polyester P(P-ItaP) prepared from two nonsymmetric phosphorus-containing comonomers also results in complex spectra. The ^{1}H NMR spectrum cannot be analyzed in detail because of extensive signal overlap (Figure S5, Supporting Information) but in the ^{13}C NMR spectrum most signals can be assigned (Figure S6, Supporting Information). The spectrum confirms the expected polymer structure and signals of low intensity can unequivocally be assigned to expected glycol ether and methyl ester end groups. In the ^{31}P NMR spectrum (Figure 2c), two signal regions can be distinguished resulting from the alkylated DOPO unit (ItaP; 36–34.8 ppm) and from the arylated DOPO (P) unit (P; 20.2 ppm). Only the latter signals showed a complex splitting resulting from the effect of the diastereomers but also from orientation of head and tail groups (regioregularity) and/or stereosequences.

3.3. Melting and Softening Behavior of the Polyesters

The glass transition temperatures T_g were determined by DSC (second heating run) and are summarized in wwt. The polyesters with ItaP units were amorphous due to steric hindrance for crystallization by the large DOPO substituents as reported before for other DOPO-substituted polyesters.[9,19,20] The T_g of the polyesters with ItaP comonomer were higher than those without phosphorus substituent and raised from the ones with short aliphatic diyl units to the aromatic one due to the sterically hindered groups in the aromatic polyester. The two DOPO groups in P(P-ItaP) resulted in high steric hindrance and restricted chain mobility, and therefore, a higher T_g of 125 °C. This temperature is closer to the T_g of P(P-T) (145 °C) with DOPO-HQ-GE units due to the aromatic rings in the backbone. P(B-Seb) had a low T_g of −53 °C due to the long aliphatic chain in the backbone. Replacement of the butane diyl unit by the DOPO-diyl unit (P) generally yielded a drastic increase of T_g to 63 °C.

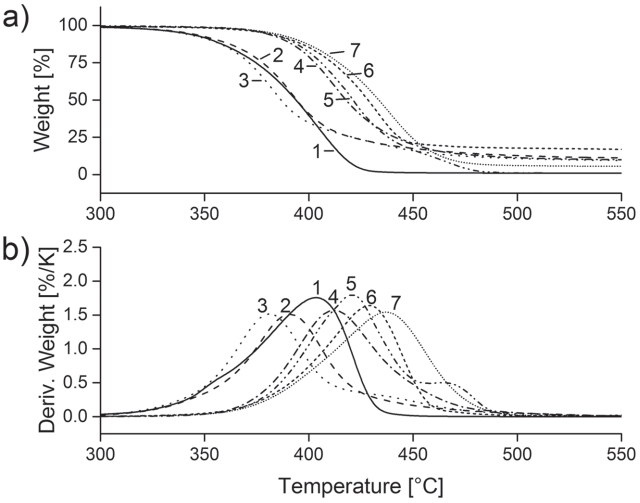

Figure 3. Thermogravimetric investigation of the polyesters obtained with a heating rate of 10 K min^{-1}; a) TGA curves; b) first derivative of mass loss curves; 1: PBS; 2: P(E-ItaP); 3: P(B-ItaP); 4: P(P-ItaP); 5: P(B-Seb); 6: P(P-Seb); 7: P(B_{30}/P_{70}-Seb).

3.4. Thermal Decomposition of PBS and P(B-Seb)

The thermal decomposition of all the polyesters was examined by TGA under nitrogen, TGA-FTIR, and Py-GC/MS. Starting with the study of PBS and P(B-Seb), the further influence of DOPO-substituents on the decomposition was explored. **Figure 3** summarizes the TGA curves and the first derivative curves of the mass loss versus temperature under nitrogen at a heating rate of 10 K min^{-1} for all polyesters.

The TGA curve of PBS (Figure 3, curve 1) and the position of the temperature at which maximum decomposition occurred (401 °C) are similar to data previously reported.[34] The authors proposed a two-step decomposition based on measurements with different heating rates. The first step with less weight loss appearing as shoulder before the main maximum was described as autocatalytic process, and the second (here at 401 °C) as main decomposition. A similar behavior was observed in this study for P(B-Seb) (Figure 3, curve 5). The curve of P(B-Seb) indicated a two-step decomposition with maxima found at 419 and 463 °C, respectively, at higher temperature than for PBS.

The nonsubstituted aliphatic polyesters decomposed nearly completely as observed earlier.[9] The composition of the gases

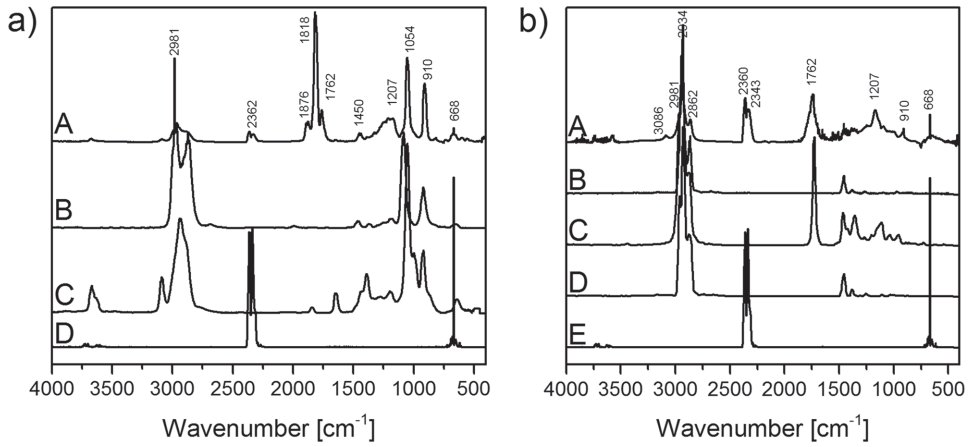

Figure 4. TGA-FTIR gas phase spectra taken during the degradation of a) PBS: (A) PBS at the main decomposition stage (37 min, 405 °C), (B) reference spectrum of tetrahydrofuran, (C) reference spectrum of 3-buten-1-ol, (D) reference spectrum of carbon dioxide, and b) P(B-Seb): (A) P(B-Seb) at the main decomposition stage (38 min, 420 °C), (B) reference spectrum of methylcyclohexane, (C) reference spectrum of 3-nonanone, (D) reference spectrum of 1,4-dimethylcyclohexane, (E) reference spectrum of carbon dioxide.

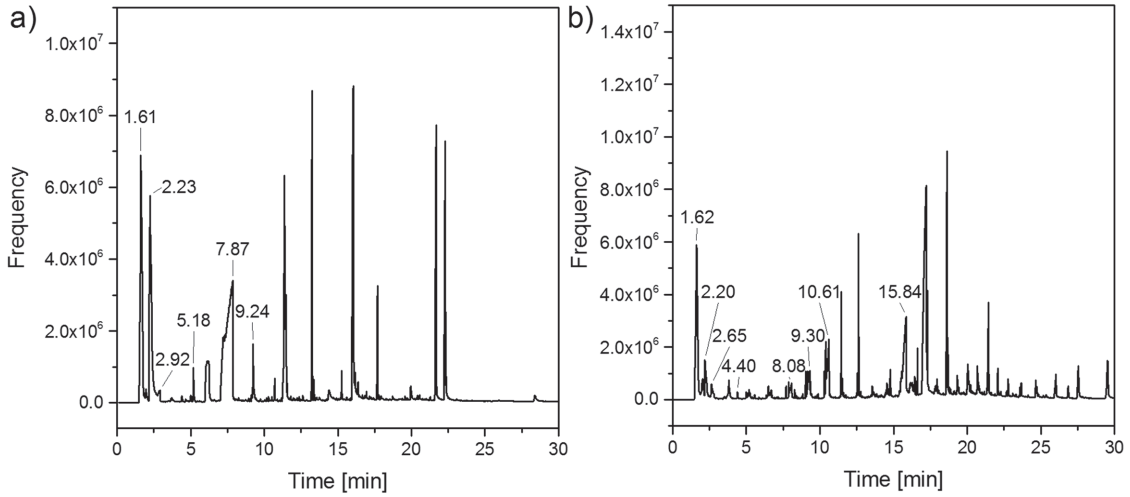

Figure 5. Pyrograms at 600 °C of a) PBS and b) P(B-Seb).

evolved at the main decomposition maximum was studied by TGA-FTIR. Py-GC/MS measurements revealed the kind of gases evolved at pyrolysis. **Figure 4** shows the TGA-FTIR spectra of the gases evolved from PBS (Figure 4a) and P(B-Seb) (Figure 4b) in TGA taken at the decomposition maxima at 405 and 420 °C, respectively. The decomposition gases of PBS contained mainly CO_2 (2362 cm^{-1}), tetrahydrofuran (THF) (2980 cm^{-1}), and 3-butene-1-ol. Further identification of gases not assignable in TGA-FTIR was performed by Py-GC/MS (**Figure 5**). Pyrolysis of PBS at 600 °C identified butadiene (BD), tetrahydrofuran, succinic anhydride, propenoic acid, propionic acid, and propyl propionate as main components. The decomposition gases of P(B-Seb) evolved at 420 °C, the temperature of the first maximum of the TGA weight loss curve, were analyzed as well. The FTIR spectrum shown in Figure 4b indicated the generation of CO_2, dimethyl sebacate (1730 cm^{-1}), 3-nonanone, methylcyclohexane, 1,4-dimethylcyclohexane, and THF. Additional Py-GC/MS (Figure 5b) at 600 °C detected BD, THF caused by ring closure of the 1,4-butanediol, together with a number of carboxylic acids (mainly sebacic acid, nonanoic acid, octanoic acid, hepanoic acid), heptane, and cyclic compounds like vinylcyclohexene. The complete content of the pyrolysis gases of PBS and P(B-Seb) is given in Table S1 (Supporting Information).

The decomposition pathways were derived from all the data obtained applying the same method as previously reported,[35] and are illustrated in **Figure 6**. Literature reports on PBS so far dealt either with thermo-oxidative processes[36] or did not illustrate the complete decomposition pathway.[34] The decomposition of PBS (Figure 6a) starts with β-hydrogen transfer as known from other polyesters and results in the formation of BD and succinic acid. Recombination with C1 radicals forms dimethylsuccinate. BD is formed successively from THF or butane-1-ol. The pathway explains the complete decomposition of PBS into combustible gases. The same was found for P(B-Seb) (Figure 6b). Comparably to PBS, P(B-Seb) forms THF and BD as well as dicarboxylic acids via β-hydrogen transfer. Sebacic acid formed initially decomposes subsequently to

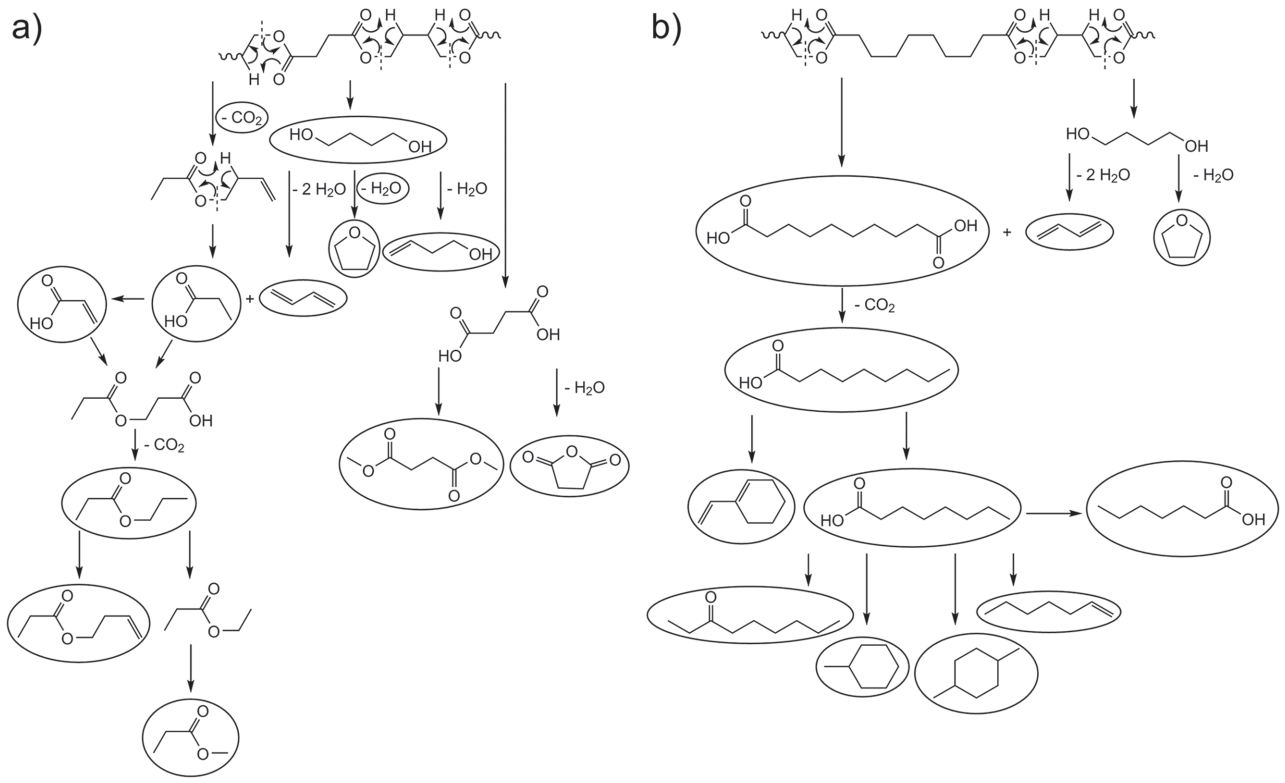

Figure 6. Decomposition pathways outlined for a) PBS and b) P(B-Seb) (framed structures = proved decomposition products in the gas phase).

CO_2, nonanoic acid, octanoic acid, hepanoic acid, and cyclics, again leaving almost no remaining residue. The subsequent decomposition of sebacic acid is regarded as reason for the two-step decomposition curve found in TGA.

3.5. Thermal Decomposition of the Phosphorus-Containing Polyesters

The phosphorus polyesters were analyzed using the same methodology as used for PBS and P(B-Seb) to explore the influence of the ItaP unit on the decomposition pathways.

TGA (see Figure 3) revealed that introduction of ItaP shifted the maximum of decomposition (maximum in the first derivative of weight loss curves) to lower temperature (in P(E-ItaP) and P(B-ItaP)) compared to PBS. Combination with the DOPO-diol in P(P-ItaP) shifted the maximum to higher temperature and resulted in an increased amount of residue.

The TGA-FTIR measurements were performed at the main decomposition maximum at 388 °C (P(B-ItaP)), respectively, 405 °C (P(P-ItaP)) (**Figure 7**). The TGA-FTIR spectrum of the gases evolved from P(B-ItaP) (Figure 7a) contained phthalic anhydride (1789 cm^{-1}), THF (2981 and 1118–907 cm^{-1}), 1,4-butanediol, 1-butene, and CO_2 (2360 cm^{-1}). Additionally, investigations of the gases were performed using Py-GC/MS (**Figure 8**a). The pyrolysis compounds found for P(B-ItaP) are BD, THF, and aromatic compounds like 2-phenylphenol and fluorene derivatives.

The TGA-FTIR spectrum of P(P-ItaP) at 405 °C (Figure 7b) shows the same bands for carbon dioxide and phthalic anhydride compared to P(B-ItaP). Furthermore, carbon monoxide (2000–2200 cm^{-1}) and acetaldehyde with additional bands (1740–1770 cm^{-1}) were detected. In the mass spectra obtained from Py-GC/MS (600 °C, Figure 8b), acetaldehyde, phenol, succinic anhydride, benzochinone, fluorene, and anthracene derivatives and DOPO-containing compounds were found. Table S2 (Supporting Information) gives a summary of all relevant pyrolysis products evolved from P(B-ItaP) and P(P-ItaP). By comparison of the compounds found for P(B-ItaP) and P(P-ItaP) it can be noted that the decomposition products resulting from the ItaP unit were the same.

The decomposition pathway for P(B-ItaP) was deduced from the pathway of PBS and is shown in **Figure 9**. It is assumed that the first step is the same as in the decomposition pathway of P(B-ItaP) forming 1,4-butanediol, which was indeed detected by Py-GC/MS. A following dehydration reaction of the 1,4-butanediol leads to the typical formation of THF and BD via β-hydrogen transfer. The resulting DOPO-Ita decomposes either through elimination of itaconic acid and the direct release of DOPO (II) or through elimination of succinic acid and the release of DOPO (I), keeping the methylene group at the phosphorus atom. Both structures were proven by Py-GC/MS. In the following decomposition of DOPO, thermodynamic stable aromatic compounds like 2-phenylphenol, phenanthrene, and many more are generated through homolysis and recombination with C1 radicals. Additionally, methylfurandione was observed as a decomposition product of itaconic acid.

Based on the results from the Py-GC/MS and TGA-FTIR and the decomposition found for P(B-ItaP) the pathway for P(P-ItaP) was derived and the complete decomposition into

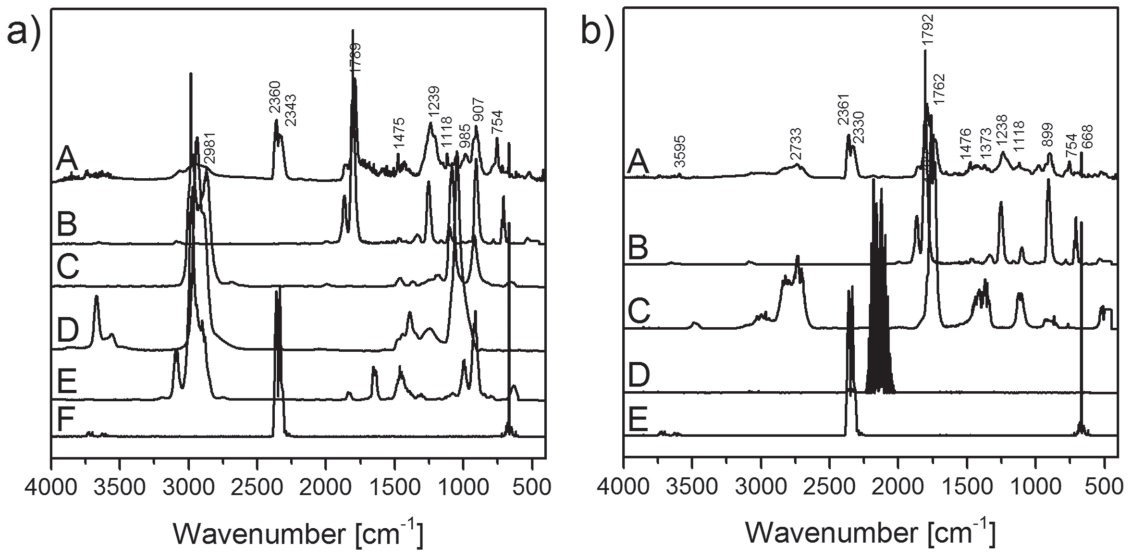

Figure 7. TGA-FTIR gas phase spectra during the degradation of a) P(B-ItaP): (A) at the main degradation stage (36 min, 388 °C), (B) reference spectrum of phthalic anhydride, (C) reference spectrum of tetrahydrofuran, (D) reference spectrum of 1,4-butanediol, (E) reference spectrum of 1-butene, (F) reference spectrum of carbon dioxide; and b) P(P-ItaP): (A) at the main degradation stage (37 min, 405 °C), (B) reference spectrum of phthalic anhydride, (C) reference spectrum of acetaldehyde, (D) reference spectrum of carbon monoxide, (E) reference spectrum of carbon dioxide.

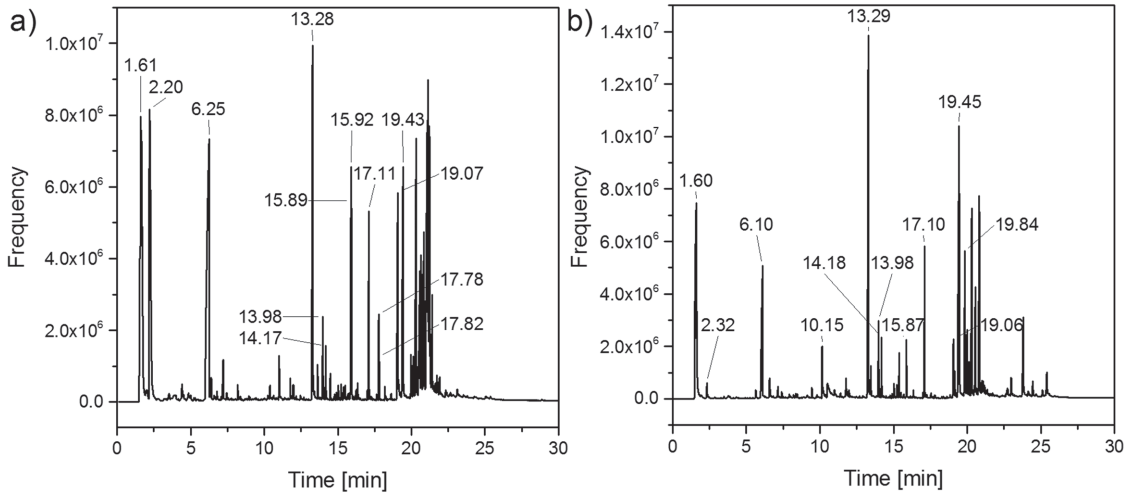

Figure 8. Mass spectra taken by pyrolysis/GC-MS after pyrolysis at 600 °C of a) P(B-ItaP) and b) P(P-ItaP).

combustible gases is shown in **Figure 10**. First, the β-hydrogen rearrangement leads to DOPO-Ita, which decomposes the same as for P(B-ItaP) and leads to the same decomposition compounds (Figure 9, dashed cycles). In addition to the gases found, decomposition products caused by the P-diyl unit were proven (acetaldehyde, phenol, and benzoquinone), which are mainly formed by β-hydrogen rearrangement resulting from DOPO-HQ-GE.

3.6. Microscale Combustion Calorimetric Results

Pyrolysis combustion flow calorimetry or MCC can serve as an orientation study for new polymer materials to evaluate the influence of changes in the polymer structure on the combustion behavior.[37,38] The pyrolysis is carried out under nitrogen. The volatile gases produced are transferred into a combustion chamber with a temperature of 900 °C and oxidized by mixing with oxygen. The rate of heat release (HRR) is monitored as function of temperature at which the volatiles are produced. The heat release capacity (HRC) is obtainable from the quotient (maximum (HRR)/heating rate), the effective heat of combustion (HOC) from heat release divided by the amount of volatiles evolved.

Figure 11 illustrates the heat release rate versus temperature curves and **Table 2** summarizes the MCC data of the polyesters studied. PBS had a maximum HRR at 407 °C. Substitution of the succinate by ItaP units in P(B-ItaP) shifted the maximum

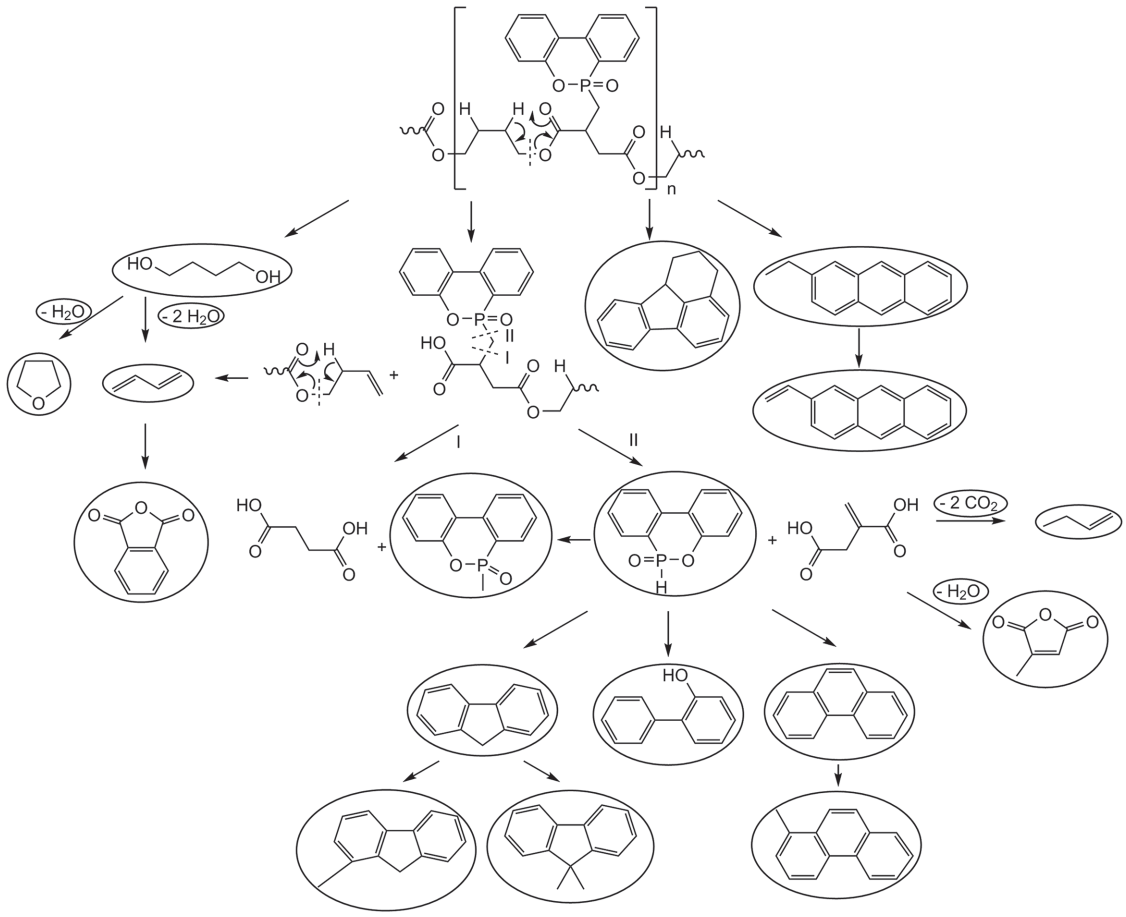

Figure 9. Thermal decomposition pathways for P(B-ItaP) (framed structures = decomposition products proven in the gas phase).

of HRR to lower temperature (404 °C). Further introduction of DOPO-diol units in P(P-ItaP) enhanced the maximum to 422 °C, close to that of P(P-T) (428 °C). The same effect was observed when the butanediol units in P(B-Seb) (T_{max} at 428 °C) were replaced by DOPO-diol units resulting in P(P-Seb) (450 °C). This can be explained by the decomposition pathway of P(B-Seb) including subsequent decomposition of decanedioic acid after its evolution at 422 °C as discussed before and shown in Figure 6b.

The data in Table 2 reflect that introduction of DOPO substituents in both the itaconate as well as sebacate polyesters reduced the HRC compared to those of PBS and P(B-Seb) controls (except for P(E-ItaP)), while HRC was significantly lowered only in the terepthalate (P(P-T)). The HOC was slightly reduced in the sebacates compared to P(B-Seb), but was increased in the P-substituted itaconate polyester compared to PBS indicating the high amount of volatiles that were generated in the decomposition and oxidized. For PBS and P(B-Seb) almost no char remained at 750 °C. In contrast, the DOPO-substituted itaconate and sebacate polyesters formed moderate char with the highest amount (13.5 wt%) for the double-substituted P(P-ItaP). However, the high char amount, low HRC, HOC, and pHRR of the terephthalate P(P-T) was not reached in the itaconate polyesters pointing out the high importance of the terephthaloyl unit for condensed phase action in polyesters.

3.7. Fire Behavior under Forced-Flaming Conditions

The burning behavior of the polyesters with altered chemical structure was studied in forced-flaming investigations in a cone calorimeter.

The HRR curves of the investigated polyesters are presented in **Figure 12**a,b. The most important results are listed in **Table 3**. The investigated polyesters can roughly be divided into two groups: pure polyesters without flame-retardant structure and flame-retarded polyesters with the phosphorus(P)-containing DOPO unit attached to their backbone. The non-flame-retarded, nonsubstituted polyesters P(B-Seb), PBS, PBT, and PET differ mainly in the structure of the main chain (aliphatic or semi-aromatic) and in the number of C and O atoms (C:O ratio) in the polymer chain due to varying lengths of the aliphatic units. Under forced-flaming conditions, P(B-Seb) and PBS burned and only formed a minor residue, PBT a rather negligible one, and PET a 9 wt% residue (Figure 12a–d).

P(B-Seb), PBS, PET, and PBT presented the typical HRR curve of noncharring materials, mainly characterized by a continuous increase in HRR after ignition until a sharp peak of HRR (PHRR) occurred at the end of combustion (Figure 12a).[30] Even though P(B-Seb), PBS, PBT, and PET are not flame-retarded, their cone calorimeter results differed strongly due to their different molecular structure. Changing

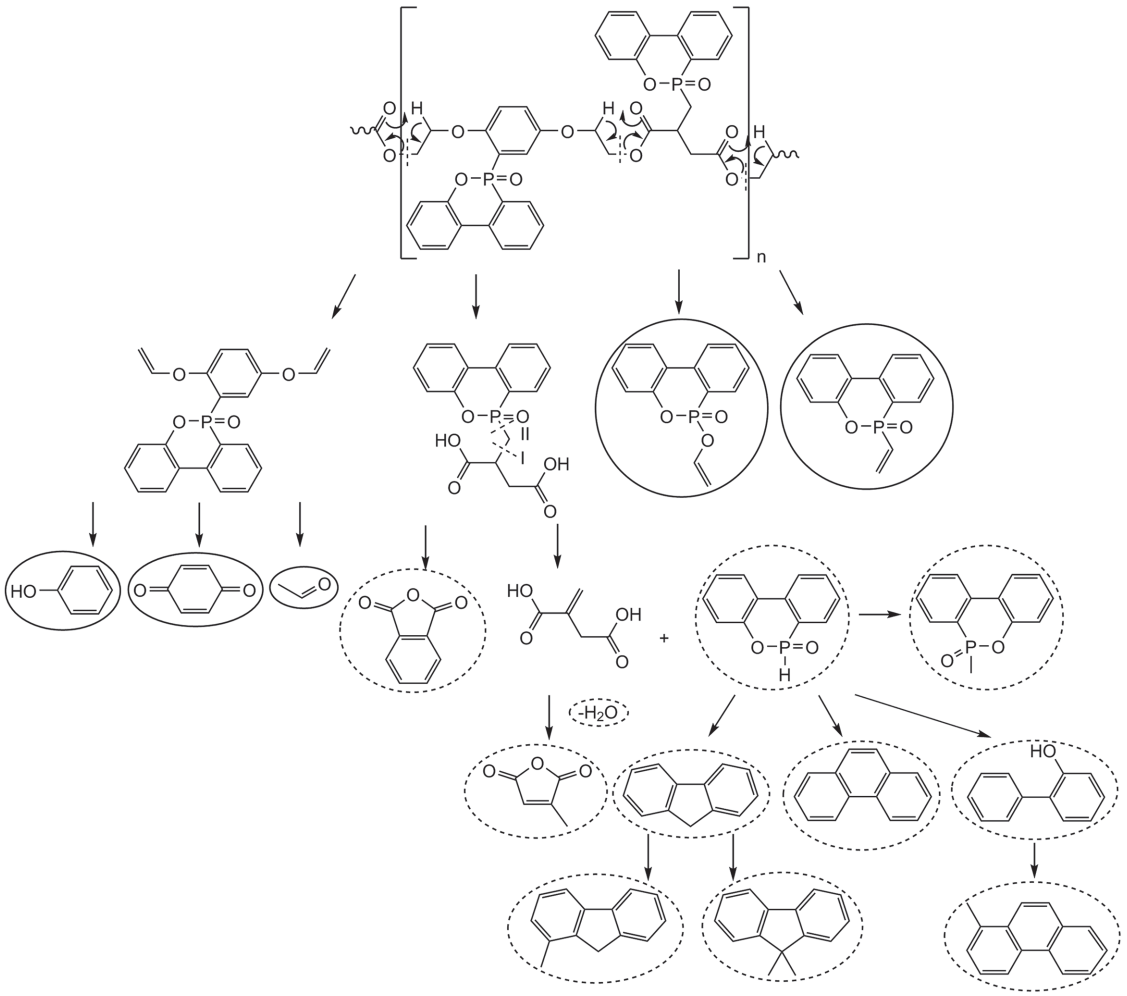

Figure 10. Thermal decomposition pathways for P(P-ItaP) (framed structures = decomposition products proven in the gas phase, dashed round frames = decomposition compounds also found for P(B-ItaP).

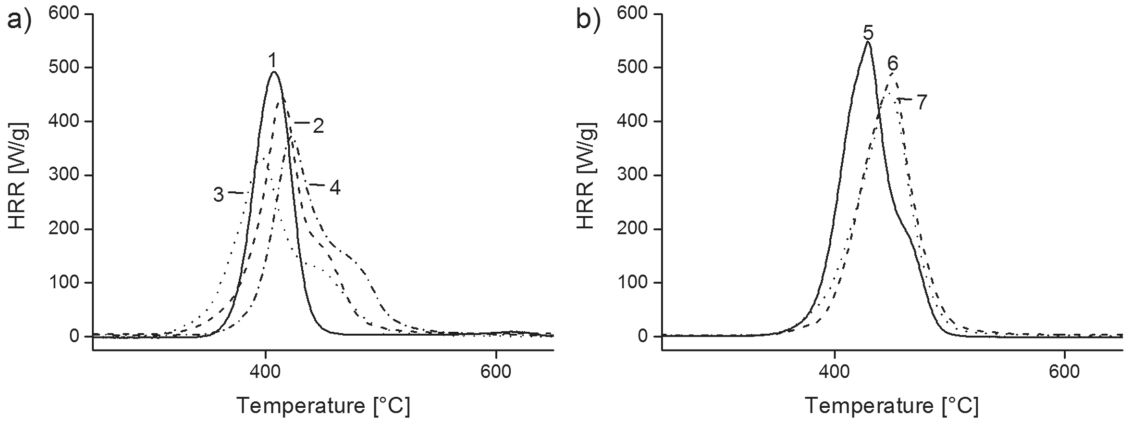

Figure 11. MCC of the polyesters obtained with a heating rate of 60 K min^{-1}; a) curves of 1: PBS and ItaP containing polyesters 2: P(E-ItaP); 3: P(B-ItaP); 4: P(P-ItaP); b) curves of sebacate polyesters 5: P(B-Seb); 6: P(P-Seb); 7: $P(B_{30}/P_{70}$-Seb).

from aliphatic to semi-aromatic backbone and decreasing C:O ratio had significant effects on the burning behavior. The most intense burning was observed for P(B-Seb) with a PHRR of 1550 kW m^{-2}, a THE of 88 MJ m^{-2} and without residue left after combustion. P(B-Seb) showed the highest C:O ratio and the H-richest aliphatic structure. With decreasing C:O ratio, the PHRR decreased for the directly comparable structures from 1550 kW m^{-2} for P(B-Seb) to 1124 kW m^{-2} for PBS, and from

Table 2. Decomposition data of the synthesized polyesters measured by MCC and TGA.

Sample	MCC					TGA	
	T_{max} [°C]	$_{max}$HR [kJ g^{-1}]	HRC [J g^{-1} K^{-1}]	HOC [kJ g^{-1}]	Char 750 °C [wt%]	T_{max} [°C]	Char 800 °C [wt%]
PBT[9]	408	21.7	512	21.61	7.7	397	8.2
PBS[9]	407	21.1	524	21.22	0.4	401	1.3
P(P-T)[28]	445/490	12.0	266	20.60	41.6	427/476	36.9
P(E-ItaP)	403	23.7	533	26.90	11.8	391	10.0
P(B-ItaP)[9]	400	24.1	407	26.23	8.1	381	8.5
P(P-ItaP)	422	23.6	495	27.32	13.5	412	8.6
P(B-Seb)	428	30.3	675	30.61	0.9	419/463	1.3
P(P-Seb)	448	27.5	578	30.61	10.3	436	5.9
P(B_{30}/P_{70}-Seb)	448	26.4	526	28.43	7.1	437	5.0

1532 kW m^{-2} for PBT to 1050 kW m^{-2} for PET. In the aliphatic polyesters, the decrease of C:O ratio from 3.5:1 for P(B-Seb) to 2.5:1 for PBS resulted in a significantly decreased effective heat of combustion (EHC) of the volatiles, whereas the increase in residue was negligible. The decrease of EHC for PET compared to PBS was the result of changing the molecular structure from aliphatic to semi-aromatic containing less H, while the C:O ratio (2.5:1) was the same for both polyesters. For the non-flame-retarded polyesters, EHC measured in the well-ventilated cone calorimeter equals the effective heat of combustion of volatiles (h_c^0). Two effects are discussed to decrease EHC of the non-flame-retarded polyesters: with decreasing C:O ratio, the release of incombustible CO_2 from polyester decomposition enhanced and thus fuel dilution effects occurred.[39] Aromatic polymers are known to have a lower h_c^0 than aliphatic ones due to the reduced H-content, so changing the polyester structure from aliphatic to semi-aromatic decreased EHC of the volatiles as well.[40] After combustion, no residue was left for aliphatic P(B-Seb) and PBS. Introduction of aromatic units in PET and PBT led to noticeable charring (**Figure 13**a–d). The lower the C:O ratio and the higher the aromaticity, the higher is the fire residue for the non-flame-retarded polyesters. The higher residue in PET is also caused by a decomposition process different from PBT. THE was decreased by both, reducing EHC which reflects the quality of the fuel released, and residue formation reducing the amount of fuel released. THE decreased in the order of P(B-Seb) > PBS > PBT > PET. In Figure 12d, THE representing the fire load is plotted against the flame spread index MARHE (maximum of averaged heat release rate) in order to access the polyesters' most important fire risks comprehensively. Compared to P(B-Seb), PBS and PBT showed

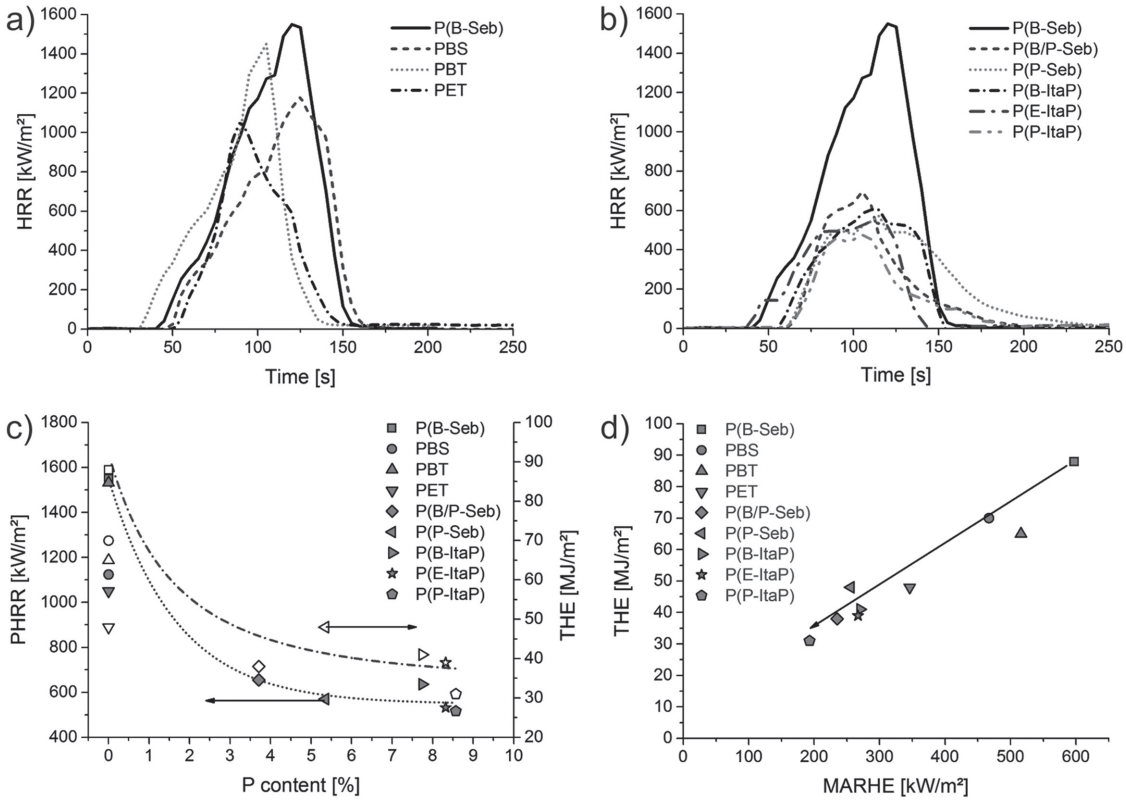

Figure 12. HRR versus time curves of a) nonsubstituted polyesters; b) DOPO-substituted polyesters; c) PHRR and THE values in dependency of the phosphorus content of the polyesters; the lines are guides to the eyes indicating the relationship between PHRR and phosphorus content; d) assessment of the polyesters fire risk by plotting fire load (THE) versus fire spread indicating MARHE; P(B/P-Seb): sample P(B_{30}/P_{70}-Seb).

Table 3. Cone calorimeter results; phosphorus content was calculated from the chemical structure; the uncertainty of the measurements was ±4% for PHRR, THE, TSR, and CO yield, ±2 s for TTI, ±1 wt% for the residue, and ±1 MJ kg^{-1} for the EHC.

Sample	P-content [%]	TTI [s]	PHRR [kW m^{-2}]	THE [MJ m^{-2}]	Residue [wt%]	EHC [MJ kg^{-1}]	TSR [m^2 m^{-2}]	CO yield [kg kg^{-1}]
P(B-Seb)	0	39	1550	88	0	28.9	871	0.0301
PBS	0	44	1124	70	0.8	21.8	394	0.0145
PBT	0	30	1532	65	2.7	20.1	1549	0.0584
PET	0	50	1050	48	9	15.6	1275	0.0579
$P(B_{30}/P_{70}$-Seb)	3.71	59	665	38	10.4	12.5	3868	0.1910
P(P-Seb)	5.35	55	570	48	10.1	15.8	4445	0.2095
P(B-ItaP)	7.74	55	636	41	7.6	12.0	5778	0.1805
P(E-ItaP)	8.32	36	532	39	10.5	11.8	5769	0.1855
P(P-ItaP)	8.57	49	516	31	14.0	9.8	5899	0.1855

a similar reduction in fire risks by reducing both measures. Among the non-flame-retarded polyesters, the smallest fire risk was observed for PET, as expected, based on the largest amount of residue and lowest effective heat of combustion. Figure 12b presents the HRR curves of DOPO-containing polyesters. The investigated DOPO-containing polyesters were again different in their aliphatic or semi-aromatic polymer backbone structures and therefore not only the P-content varied, but also the C:O ratio and H-content. With the exception of P(E-ItaP), the DOPO-substituted polyesters delayed the time to ignition (TTI) by 10–20 s compared to P(B-Seb). For P(P-Seb) and P(P-ItaP) flashing was observed prior to ignition. The PHRR of DOPO-containing polyesters was reduced by 57–67% with increasing P-content compared to P(B-Seb). After ignition, $P(B_{30}/P_{70}$-Seb), P(B-ItaP), P(E-ItaP), and P(P-ItaP) burnt as pool-fire for 100–120 s. Afterward, close to the end of

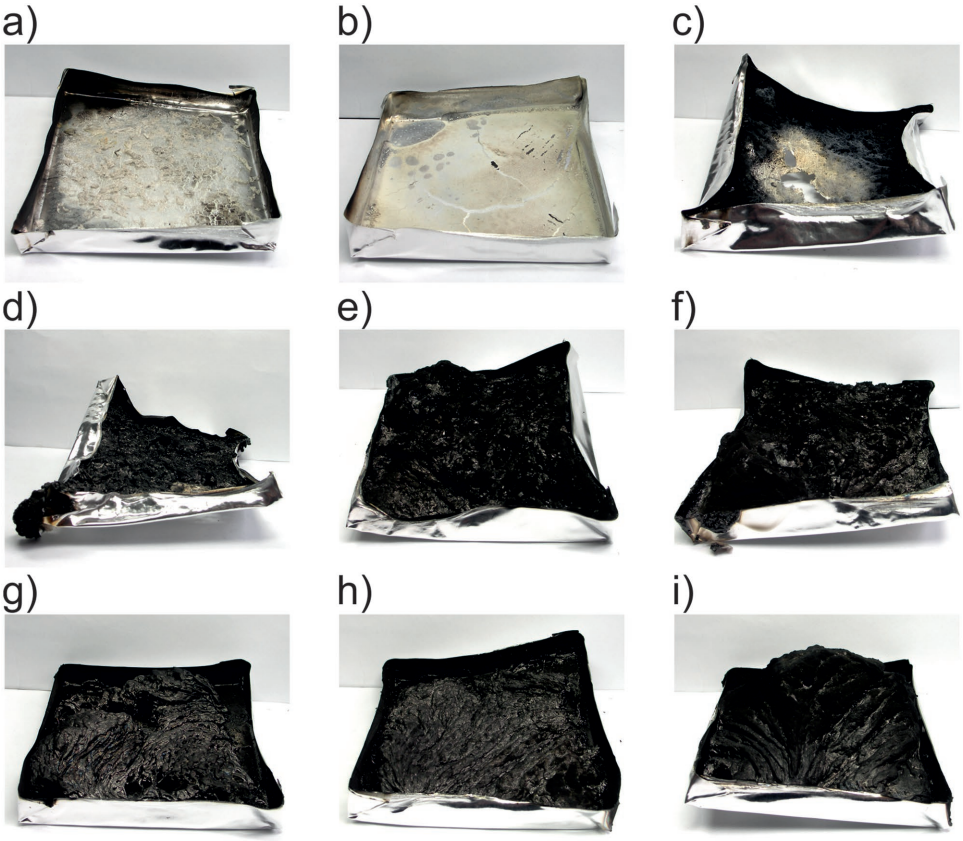

Figure 13. Cone calorimeter residues of a) P(B-Seb), b) PBS, c) PBT, d) PET, e) $P(B_{30}/P_{70}$-Seb), f) P(P-Seb), g) P(B-ItaP), h) P(E-ItaP), and i) P(P-ItaP).

combustion, a sudden formation of a swollen fire residue occurred. Only the residue formation of P(P-Seb) started earlier during combustion and proceeded slower. After combustion, the DOPO-containing polyesters left residues between 7.6 wt% (P(B-ItaP)) and 14.0 wt% (P(P-ItaP)) (Figure 13e–i). THE of the flame-retarded polyesters was reduced by 45–65% compared to P(B-Seb). As shown in Figure 12c, the relation between PHRR and P-content and between THE and P-content is non-linear and presents the highest relative reduction of PHRR and THE for lower P-content. The levelling off in the flame retardancy performance and thus much higher efficiency at low P-contents has been reported for P-containing flame retardants before.[41,42] With increasing P-content, PHRR and THE decreased further but the flame retardancy efficiency levelled off. Due to increase in TTI and reduction in HRR, the MARHE was strongly reduced for the DOPO-polyesters compared to P(B-Seb), similar to the materials' fire load THE.

With the observed flame retardancy with respect to flame spread and fire load, the fire risk of DOPO polyesters was tremendously reduced. A remarkable flame retardancy effectivity was reached with P-contents below 6 wt%. The flame retardancy effect of DOPO polyesters was accompanied by a tremendous strong increase in smoke production (TSR) by 340–580% and CO yield of ≈500% compared to P(B-Seb) (Table 3). This increase in CO yield and TSR indicated incomplete combustion due to the strong flame retardancy process occurring in the gas phase.

3.8. Assessment of Flame Retardancy Pathways

The increase in fire residue indicated a flame retardancy mode of action in the condensed phase for DOPO-containing polyesters. Figure 13 presents the residues of DOPO polyesters. The residue amounts between 7.6 and 14.0 wt% indicated charring and thus reduction in fuel released to the gas phase. Further, the significant reduction in EHC, the increase in TSR, and CO yield with increasing P-content indicated an additional flame retardancy mode of action in the gas phase **Figure 14**. While the EHC of the polyesters without DOPO equaled the effective heat of combustion of volatiles (h_C^0), the EHC of DOPO polyesters equaled the combustion efficiency (χ) multiplied by h_C^0. The decrease in EHC, as well as the increase in TSR and CO yield for DOPO polyesters indicated the suppression of complete combustion most probably due to the release of radical scavenging P species to the gas phase and therefore the reduction of χ. Decrease in EHC and increase of CO yield leveled off with increasing P-content and indicated that the gas phase effectivity of DOPO decreased at higher concentrations. This kind of leveling off has been reported before for flame inhibition by several P-containing flame retardants and is a typical effect of P-containing species in the gas phase.[41–44] DOPO polyesters with C:O ratios between 3.5:1 and 1.5:1 in the polymer backbone were investigated. With decreasing C:O ratio, the content of carboxyl groups is higher and an increasing release of incombustible CO_2 from polyester pyrolysis occurred.[12,39] The released CO_2 diluted the fuel in the gas phase and decreased h_C^0. The DOPO polyesters had mainly aliphatic backbone structures which were decomposed to aliphatic volatiles that were very similar. Thus, only a minor influence on h_C^0 was found. The high smoke and CO release indicated flame inhibition by radical scavenging to be the main gas phase flame retardancy mode of action of DOPO polyesters. Reduction of fuel due to charring and reduction of EHC due to flame inhibition and fuel dilution were both identified as flame retardancy mode of actions in DOPO polyesters. The gas phase processes with reduction in EHC of 46–57% clearly outperformed charring with residue amounts of 10–14 wt% over the whole P-content range in the DOPO polyesters investigated.

Table 3 presents the reduction of fire behavior characteristics and the quantification of the flame retardancy processes. To exclude effects of fuel dilution, polyesters with similar C:O ratios were used for the quantification keeping h_C^0 roughly constant: P(B_{30}/P_{70}-Seb) and P(P-Seb) were compared to P(B-Seb) (C:O ratio 3.4–3.5:1) and P(P-ItaP) was compared to PBS (C:O ratio 2.3–2.5:1). With constant h_C^0, the combustion efficiency χ is the only factor influencing EHC. The effect of flame inhibition and charring on the burning behavior of DOPO polyesters was quantified using Equations (1) and (2)[45]

$$\mathrm{THE} \approx \chi \cdot (1-\mu) \cdot h_C^0 \cdot m_0 \quad (1)$$

and

$$\mathrm{HRR} \approx \chi \cdot (1-\mu) \cdot h_C^0 \quad (2)$$

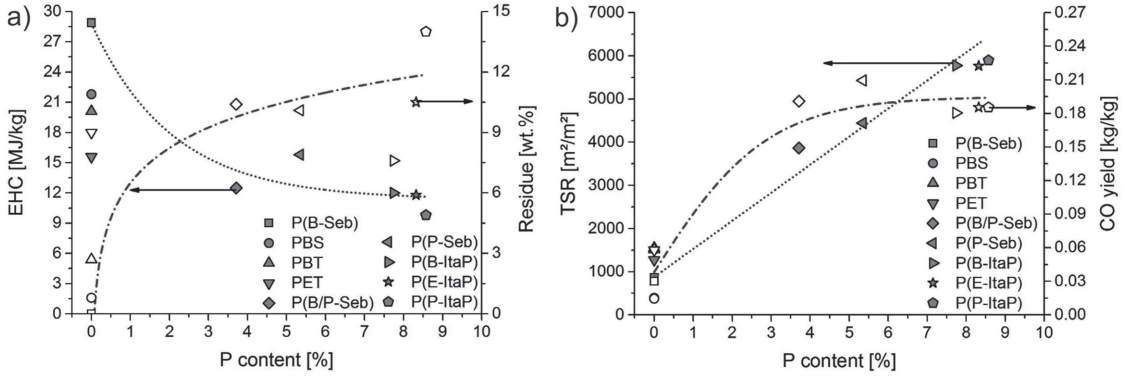

Figure 14. a) EHC and residue and b) TSR and CO yield in dependency of the polyester phosphorus content; the lines are guides to the eyes indicating the relationship between fire properties and phosphorus content; P(B/P-Seb): sample P(B_{30}/P_{70}-Seb).

Table 4. Quantification of the reduction in THE and PHRR due to the flame retardancy modes of action: charring, gas phase action, and residual protection layer for polyesters with similar C:O ratio in the backbone.

Sample	P-content [wt%]/ (C:O ratio)	Relative change in						Due to protection layer
		$1-\mu$	EHC	m_0	$(1-\mu) \times$ EHC $\times m_0$	THE	PHRR	
P(B-Seb)	0/(3.5:1)	1.000	1.000	1.000	1.000	1.000	1.000	1.000
P(B_{30}/P_{70}-Seb)	3.71/(3.4:1)	0.896	0.433	1.118	0.433	0.432	0.429	0
P(P-Seb)	5.35/(3.5:1)	0.899	0.547	1.144	0.563	0.545	0.368	0.648
PBS	0/(2.5:1)	1.000	1.000	1.000	1.000	1.000	1.000	1.000
P(P-ItaP)	8.57/(2.3:1)	0.867	0.450	1.138	0.444	0.443	0.459	0

The values given in **Table 4** of P(B-Seb) and PBS as controls were set to one, P(B_{30}/P_{70}-Seb), P(P-Seb), and P(P-ItaP) are relative values. The reduction in released fuel ($1-\mu$) and the reduction in EHC were taken from the cone calorimeter data. Compared to the aliphatic polyesters without DOPO, the density of DOPO polyesters was obviously increased indicated by the higher initial sample mass m_0 of the cone calorimeter specimen with same dimensions. As THE is the fire load of the complete specimen, the increase of m_0 has to be taken into account in order to calculate THE. In fact, the reduction of ($1-\mu$) and the increase in m_0 were in the same range of 10–14%. This indicated that the increase in sample mass fully compensated the fuel reduction due to charring. As predicted by Equation (1), the product $(1-\mu) \times$ EHC $\times\ m_0$ was reduced to the same level as THE. Regarding the fire load, DOPO polyesters were flame-retarded by flame inhibition and charring. The charring effect was compensated by the increase in DOPO polyesters density. According to Equation (2), charring and flame inhibition are also relevant flame retardancy processes for the reduction of HRR. In a first approximation, reductions in HRR and PHRR are assumed to originate from reductions in $(1-\mu)$·EHC as previously shown for P-containing flame-retarded polyesters.[12] Assuming similar thickness of the pyrolyzing zones, the HRR approximation has to be corrected by the increased material density, too. Based on this assumption, a PHRR reduction to 0.433 was expected for P(B_{30}/P_{70}-Seb) and to 0.444 for P(P-ItaP), respectively. The measured relative change in PHRR of P(B_{30}/P_{70}-Seb) and P(P-ItaP) fits well with the calculated values (Table 4).

Consequently, charring—counterbalanced by density increase—and flame inhibition were the two flame retardancy modes of action identified to decrease the PHRR of P(B_{30}/P_{70}-Seb) and P(P-ItaP). Even though there were residues left for P(B_{30}/P_{70}-Seb) and P(P-ItaP) at the end of combustion, these residues did not function as protection layers during combustion reducing the HRR, for example, intumescence was not observed as in the case of P(P-T). This conclusion is in agreement with the visual observation during the fire test. The P(B_{30}/P_{70}-Seb) and P(P-ItaP) residues did not develop until the end of combustion process so that both polyesters presented pool-fire burning of a liquid for most of the cone calorimeter testing time. Flame retardancy due to a protective layer was not identified for most of the DOPO polyesters investigated. P(P-Seb) was the only DOPO polyester with protection layer formation during burning and a HRR curve that came close to the typical HRR curves of charring materials.[30] In the case of P(P-Seb), a relative PHRR of 0.563 was expected by flame inhibition and charring, but a much lower relative PHRR of 0.368 was measured. This additional reduction of PHRR was caused by the fire residue that worked as effective protection layer. Taking the protection layer into account as third flame retardancy mode of action in addition to charring and gas phase activity, the reduction in PHRR due to the protection layer was around 35% for P(P-Seb). Thus, in terms of PHRR the protection layer became a major mode of action beside flame inhibition. For all the DOPO-containing polyesters investigated, flame inhibition was identified as the main flame retardancy mode of action.

4. Conclusions

Aliphatic polyesters with DOPO-substituted itaconyl units were synthesized and their thermal decomposition was examined in detail and correlated to the fire behavior. A DOPO-containing diol as well as DOPO-substituted itaconic acid were employed and the influence on decomposition and burning was elaborated. Using both DOPO-containing monomers resulted in a new polyester with two DOPO substituents per repeating unit. The results obtained were also compared to the terephthalate polyester with DOPO-diyl units (P(P-T)).

Combination of TGA, TGA-FTIR, and pyrolysis GC/MS showed that the residue left after thermal decomposition enhanced with increasing aromatic content. The residue was always significantly lower than for the terephthalate polyester P(P-T). The incorporation of terephthaloyl units generally led to higher char amounts. This is explained by different decomposition pathways of terephthalate polyesters and itaconate polyesters. In both types primary scission of ester bonds occurs yielding terminal vinylether and COOH groups, followed by evolution of acetaldehyde. In the presence of terephthaloyl units, the recombination of remaining aromatic radicals generated an aromatic char. Itaconyl polyesters decomposed into more volatiles that were evolved in the gas phase. The incorporation of a longer aliphatic chain in P(P-Seb) led to a two-step decomposition. The use of two DOPO-units contributed to a significant increase of char compared to P(B-ItaP), but did not reach the value of P(P-T), and to a change in the pyrolysis products in the gaseous phase.

The decomposition pathways of P(B-ItaP) and P(P-ItaP) based mainly on β-hydrogen transfer as first step, as it is typical for polyesters. For P(P-ItaP), an intramolecular rearrangement between ItaP- and DOPO-diyl units was observed. Py-GC/MS, TGA-FTIR, TGA, and MCC gave strong indications for a dominant gas phase action of the ItaP polyesters.

This result was verified in forced-flaming examinations in the cone calorimeter. The studied DOPO-containing polyesters showed flame inhibition as the major mode of action for flame

retardancy. Flame inhibition was visible by increased smoke release indicating incomplete burning. Besides gas phase action, charring was observed in P(P-ItaP) and P(B_{30}/P_{70}-Seb) as well, resulting in the reduction of PHRR and MARHE, and thus, combustibility. Flame retardancy due to the generation of a protective layer as observed in the terephthalate-based polyester P(P-T)[8,13,16] was only detected in the sebacate polyester with DOPO-diyl units (P(P-Seb)), combining now three modes of action (gas phase, charring, and intumescence) yielding PHRR reduced to 35%. The polyester with two DOPO units (P(P-ItaP)) showed the highest flame retardant effect indicated by high char formation, reduction of time-to-ignition, and low fire load. This is due to the combination of both high aromatic content and enhanced phosphorus content.

In summary, it is noted that the present study allows selecting candidates as polymeric flame-retardant additives for aliphatic polyesters, in particular PBS. Results for the efficacy in PBS have already been obtained but will be published separately. The high gas phase activity of the materials also suggests application of the new materials in polyester foams.

Supporting Information

Supporting Information is available from the Wiley Online Library or from the author.

Acknowledgements

The authors would like to thank co-workers from IPF Dresden for valuable contributions: Mrs. K. Arnhold for TGA and TGA-FTIR investigations, Mrs. P. Treppe for SEC measurements, and Mrs. E. Schierz for Py-GC/MS investigations.

Conflict of Interest

The authors declare no conflict of interest.

Keywords

biobased polyesters, fire behavior, flame retardance, phosphorus-containing polyesters, pyrolysis

Received: October 11, 2017
Revised: November 13, 2017
Published online: December 27, 2017

[1] R. Mülhaupt, *Macromol. Chem. Phys.* **2013**, *214*, 159.
[2] D. S. Achilias, A. Chondroyiannis, M. Nerantzaki, K.-V. Adam, Z. Terzopoulou, G. Z. Papageorgiou, D. N. Bikiaris, *Macromol. Mater. Eng.* **2017**, *302*, 1700012.
[3] G. Coativy, M. Misra, A. K. Mohanty, *Macromol. Mater. Eng.* **2017**, *302*, 1600294.
[4] G. V. N. Rathna, B. S. T. Gadgil, N. Killi, in *Biodegradable and Biobased Polymers for Environmental and Biomedical Applications* (Eds: S. Kalia, L. Avérous), John Wiley & Sons, Inc., Hoboken, NJ, USA **2016**, p. 25.
[5] C. W. Lee, C. Na, Y. Kimura, K. Masutani, *Macromol. Mater. Eng.* **2016**, *301*, 1121.
[6] Y. Ichikawa, T. Mizukoshi, in *Synthetic Biodegradable Polymers* (Eds: B. Rieger, A. Künkel, G. W. Coates, R. Reichardt, E. Dinjus, T. A. Zevaco), Springer, Berlin **2012**, p. 285.
[7] J. Xu, B.-H. Guo, *Biotechnol. J.* **2010**, *5*, 1149.
[8] A. Käppler, D. Fischer, S. Oberbeckmann, G. Schernewski, M. Labrenz, K.-J. Eichhorn, B. Voit, *Anal. Bioanal. Chem.* **2016**, *408*, 8377.
[9] D. Pospiech, A. Korwitz, H. Komber, D. Jehnichen, L. Haussler, H. Scheibner, M. Liebmann, K. Jahnichen, B. Voit, *Macromol. Chem. Phys.* **2015**, *216*, 1447.
[10] J. Troitzsch, *Plastics Flammability Handbook*, Hanser, München, Germany **2004**.
[11] S. V. Levchik, E. D. Weil, *Polym. Int.* **2005**, *54*, 11.
[12] S. Brehme, B. Schartel, J. Goebbels, O. Fischer, D. Pospiech, Y. Bykov, M. Döring, *Polym. Degrad. Stab.* **2011**, *96*, 875.
[13] E. Gallo, B. Schartel, U. Braun, P. Russo, D. Acierno, *Polym. Adv. Technol.* **2011**, *22*, 2382.
[14] T. Köppl, S. Brehme, D. Pospiech, O. Fischer, F. Wolff-Fabris, V. Altstädt, B. Schartel, M. Döring, *J. Appl. Polym. Sci.* **2013**, *128*, 3315.
[15] U. Braun, H. Bahr, H. Sturm, B. Schartel, *Polym. Adv. Technol.* **2008**, *19*, 680.
[16] Y.-L. Chang, Y.-Z. Wang, D.-M. Ban, B. Yang, G.-M. Zhao, *Macromol. Mater. Eng.* **2004**, *289*, 703.
[17] L. M. de Espinosa, M. A. R. Meier, J. C. Ronda, M. Galià, V. Cádiz, *J. Polym. Sci., Part A: Polym. Chem.* **2010**, *48*, 1649.
[18] O. Petreus, T. Vlad-Bubulac, C. Hamciuc, *Eur. Polym. J.* **2005**, *41*, 2663.
[19] O. Fischer, D. Pospiech, A. Korwitz, K. Sahre, L. Häußler, P. Friedel, D. Fischer, C. Harnisch, Y. Bykov, M. Döring, *Polym. Degrad. Stab.* **2011**, *96*, 2198.
[20] D. Pospiech, D. Jehnichen, H. Komber, A. Korwitz, A. Janke, T. Hoffmann, B. Kretzschmar, L. Häussler, U. Reuter, M. Döring, S. Seibold, R. Perez-Graterol, J. K. W. Sandler, V. Altstädt, F. Bellucci, G. Camino, *J. Nanostruct. Polym. Nanocompos.* **2008**, *4*, 62.
[21] L. Chen, C. Ruan, R. Yang, Y.-Z. Wang, *Polym. Chem.* **2014**, *5*, 3737.
[22] J.-B. Zhang, X.-L. Wang, Q.-X. He, H.-B. Zhao, Y.-Z. Wang, *Polym. Degrad. Stab.* **2014**, *108*, 12.
[23] X.-C. Bian, L. Chen, J.-S. Wang, Y.-Z. Wang, *J. Polym. Sci., Part A: Polym. Chem.* **2010**, *48*, 1182.
[24] S. Brehme, T. Köppl, B. Schartel, O. Fischer, V. Altstädt, D. Pospiech, M. Döring, *Macromol. Chem. Phys.* **2012**, *213*, 2386.
[25] S. Endo, T. Kashihara, A. Osako, T. Shizuki, T. Ikegami, (T.S. Co.), *US 4,157,436*, **1979**.
[26] S. Endo, T. Kashihara, A. Osako, T. Shizuki, T. Ikegami, (T.S. Co.), *US 4,127,590*, **1978**.
[27] C. S. Wang, C. H. Lin, *Polymer* **1999**, *40*, 747.
[28] O. Fischer, *Ph.D. thesis*, Technische Universität Dresden **2013**.
[29] B. Schartel, M. Bartholmai, U. Knoll, *Polym. Degrad. Stab.* **2005**, *88*, 540.
[30] B. Schartel, T. R. Hull, *Fire Mater.* **2007**, *31*, 327.
[31] C.-H. Chen, J.-S. Peng, M. Chen, H.-Y. Lu, C.-J. Tsai, C.-S. Yang, *Colloid Polym. Sci.* **2010**, *288*, 731.
[32] C.-H. Zhang, M. Zhang, X. Zhao, *Mod. Chem. Ind.* **2008**, *10*, 014.
[33] Z. Wei, C. Zhou, Y. Yu, Y. Li, *Polymer* **2015**, *71*, 31.
[34] K. Chrissafis, K. M. Paraskevopoulos, D. N. Bikiaris, *Thermochim. Acta* **2005**, *435*, 142.
[35] B. Schartel, B. Perret, B. Dittrich, M. Ciesielski, J. Krämer, P. Müller, V. Altstädt, L. Zang, M. Döring, *Macromol. Mater. Eng.* **2016**, *301*, 9.
[36] P. Rizzarelli, S. Carroccio, *Polym. Degrad. Stab.* **2009**, *94*, 1825.
[37] B. Schartel, C. A. Wilkie, G. Camino, *J. Fire Sci.* **2016**, *34*, 447.
[38] R. E. Lyon, R. N. Walters, *J. Anal. Appl. Pyrolysis* **2004**, *71*, 27.

[39] S. V. Levchik, E. D. Weil, *Polym. Adv. Technol.* **2004**, *15*, 691.
[40] R. N. Walters, S. M. Hackett, R. E. Lyon, *Fire Mater.* **2000**, *24*, 245.
[41] K. Langfeld, A. Wilke, A. Sut, S. Greiser, B. Ulmer, V. Andrievici, P. Limbach, M. Bastian, B. Schartel, *J. Fire Sci.* **2015**, *33*, 157.
[42] S. Rabe, Y. Chuenban, B. Schartel, *Materials* **2017**, *10*, 455.
[43] S. Brehme, T. Köppl, B. Schartel, V. Altstädt, *e-Polymers* **2014**, *14*, 193.
[44] G. F. Levchik, S. V. Levchik, G. Camino, E. D. Weil, *Fire Retardancy of Polymers*, Woodhead Publishing, Oxford **1998**, p. 304.
[45] R. E. Lyon, in *Handbook of Building Materials for Fire Protection* (Ed: C. Harper), McGraw-Hill, New York **2004**, p. 3.1.